BRAIN RESEARCH

Prospective representation of navigational goals in the human hippocampus

Thackery I. Brown,[1]* Valerie A. Carr,[1,2] Karen F. LaRocque,[1] Serra E. Favila,[3] Alan M. Gordon,[1] Ben Bowles,[4] Jeremy N. Bailenson,[5] Anthony D. Wagner[1,6]*

Mental representation of the future is a fundamental component of goal-directed behavior. Computational and animal models highlight prospective spatial coding in the hippocampus, mediated by interactions with the prefrontal cortex, as a putative mechanism for simulating future events. Using whole-brain high-resolution functional magnetic resonance imaging and multi-voxel pattern classification, we tested whether the human hippocampus and interrelated cortical structures support prospective representation of navigational goals. Results demonstrated that hippocampal activity patterns code for future goals to which participants subsequently navigate, as well as for intervening locations along the route, consistent with trajectory-specific simulation. The strength of hippocampal goal representations covaried with goal-related coding in the prefrontal, medial temporal, and medial parietal cortex. Collectively, these data indicate that a hippocampal-cortical network supports prospective simulation of navigational events during goal-directed planning.

Prospective thought and the simulation of future experiences are fundamental for planning how to best achieve immediate and longer-term goals. Prospection is theorized to rely on neural mechanisms that underlie episodic memory (*1*, *2*), drawing on declarative memory for distinct events to flexibly simulate future experiences and outcomes. The hippocampus subserves episodic retrieval of goal-relevant spatial sequences in rodents (*3*–*7*) and humans (*8*–*12*) and plays a central role in models of goal-directed navigation and episodic memory (*13*–*15*). In rodents, hippocampal "place cells" exhibit prospective sequential firing along navigational routes during planning that reflects current goals (*16*, *17*). Prospective firing may support reinstatement of the multifeatural representations of spatial contexts in a broader network underlying prospection and goal coding [including the medial temporal lobe (MTL), retrosplenial complex (RSC), and ventral striatum (VS)] (*1*, *2*, *18*–*21*). Prospective simulation may also rely on hippocampal interactions with the prefrontal cortex (PFC), which may provide cognitive control machinery through which mnemonic details are flexibly accessed and combined into the formulation of future route plans (*22*, *23*). A fundamental question in human cognitive neuroscience is whether the hippocampus and its functional interactions support flexible prospective representation of spatial trajectories during goal-directed planning.

Although human hippocampal neurons demonstrate location- and goal-related responses that can be reinstated during retrieval (*24*, *25*), noninvasive quantification of the neural representation of spatial information in humans is a challenge. Functional magnetic resonance imaging (fMRI) has revealed distance-to-goal (*26*–*28*) and grid cell–like (*29*) response coding in the human hippocampus and entorhinal cortex. Measurement of purely place cell–based location codes may not be feasible with fMRI; however, it may be possible to quantify episodic retrieval of a distributed multifeatural engram of a spatial context. Multivariate fMRI approaches have demonstrated that distributed patterns in the hippocampus, MTL cortex, and RSC carry representational information about environmental features, locations, and the direction to a goal (*30*–*34*). However, direct evidence that this hippocampal-cortical network supports prospective goal coding during route planning in humans has yet to be shown.

We used whole-brain high-resolution fMRI (hr-fMRI; 1.6-mm isotropic voxels) to simultaneously record fine-grained pattern information from the human hippocampus and a core network of anatomically and functionally interconnected regions putatively involved in goal coding and prospection (supplementary materials). Participants underwent hr-fMRI while performing a virtual navigation paradigm designed to parallel tasks that have been used with rodents (*17*, *35*). On day 1, outside the scanner, participants learned to navigate to five goal locations in a virtual circular environment, each marked by a distinct pair of fractal images (Fig. 1, A and B). On day 2, while undergoing hr-fMRI, participants began each trial at one of the locations; their viewpoint then shifted toward the ground, and they were cued with one of the fractals to plan navigation of the shortest route from their current position to the cued goal location (planning period). The participant's view then panned up, and they actively navigated to the goal. Critically, fractals were no longer visible at the goal locations on day 2, and thus performance depended on memory (Fig. 1C). During scanning, participants planned and executed navigation between the five locations across 160 trials (32 per location, visiting every location from every other location an equal number of times). This design enabled analysis of neural patterns during planning that represent information about future goal states—information that generalizes across cues, start positions, and routes.

We used multi-voxel pattern analyses to classify planning period activity (before active navigation) as being related to the current location ("current" classifier) or the future goal location to which participants would navigate ("future" classifier). We quantified current-state and future goal–state representations and their relative strength on a region-by-region and trial-by-trial basis by using classifier accuracy (significance measured against empirically validated chance; supplementary materials) and probabilistic evidence scores. In hypothesis-driven analyses, we analyzed data from a priori anatomical regions of interest (ROIs). We indexed the representation of navigational events within the hippocampus and examined how hippocampal representations covary with (i) goal-related codes in the MTL cortex, RSC, and VS and (ii) planning activity in the PFC.

On day 2, participants were highly accurate at cued navigation, performing near ceiling levels (supplementary materials). Applying the "current" classifier to the planning period data, we confirmed that distributed patterns of human hippocampal activity code for current location (classifier accuracy, 29.9%; $t_{16} = 5.55$, $P = 4.40 \times 10^{-5}$; see the supplementary materials for additional details and classification in extrahippocampal ROIs).

Turning to our first central question, we used the "future" classifier to characterize patterns during planning that carry information about future goal locations. Distributed hippocampal activity patterns during planning carried information that significantly distinguished future goal states (classifier accuracy, 29.4%; $t_{16} = 7.54$, $P = 1.19 \times 10^{-6}$) (Fig. 2A). By using neural activity measured during the planning period to classify future goal states, our principal analyses controlled for the contribution of unwanted perceptual and cognitive factors. Specifically, the classification analyses of the planning period targeted representational information that was separated in time from the perception of any past or present goal locations. Consistent with the finding that, in rodents, prospective hippocampal coding for a given location involves reinstatement of the same neural patterns that are present during experience at that location (*17*), a follow-up analysis provided evidence that reinstatement of neural patterns associated with goal arrival occurs during, and contributes to, goal coding during navigational planning (this and other supporting analyses are described in the supplementary materials).

[1]Department of Psychology, Stanford University, Stanford, CA, USA. [2]Department of Psychology, San Jose State University, San Jose, CA, USA. [3]Department of Psychology, New York University, New York, NY, USA. [4]Department of Psychology, University of California–Berkeley, Berkeley, CA, USA. [5]Department of Communication, Stanford University, Stanford, CA, USA. [6]Neurosciences Program, Stanford University, Stanford, CA, USA.
*Corresponding author. Email: thackery@stanford.edu (T.I.B.); awagner@stanford.edu (A.D.W.)

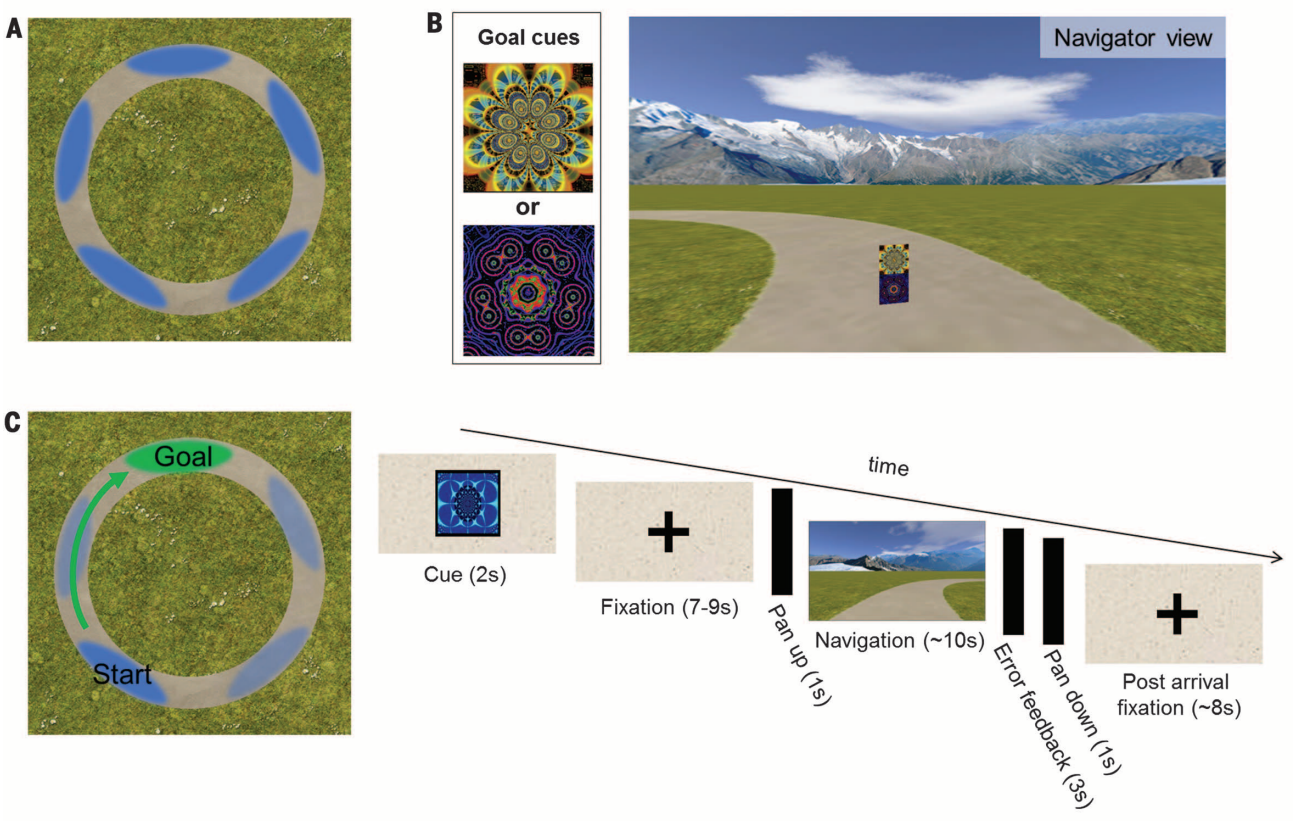

Fig. 1. Task design. (**A**) Overhead view of goal locations (illustrated by blue ellipses) in the virtual environment. (**B**) Example pair of fractals (left) and how fractals appeared at goal locations during day 1 training (right). Fractals were not visible at the locations during day 2 testing. (**C**) Test trial structure. Participants began at one familiar location (blue ellipse), were presented a goal fractal as a cue, and then planned (cue plus fixation periods) and executed navigation to the goal (green ellipse).

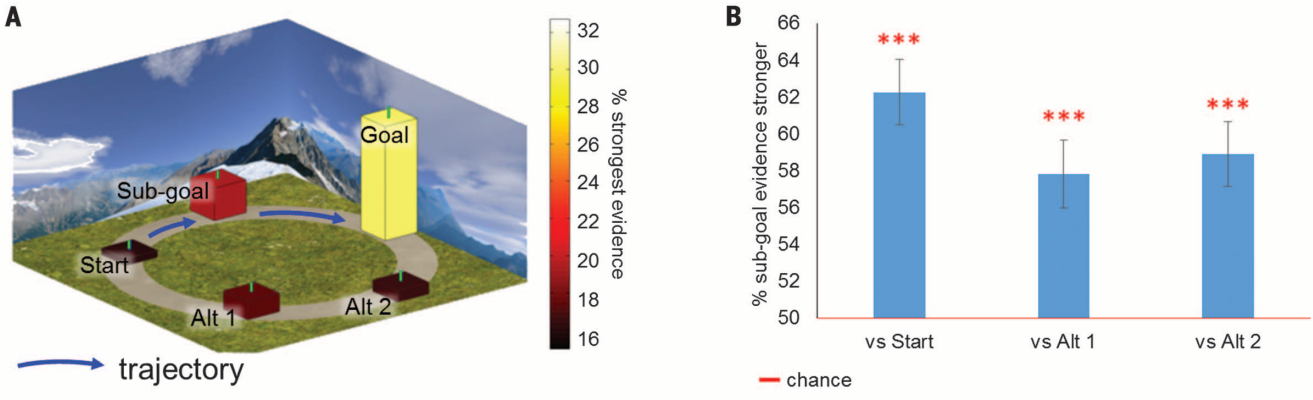

Fig. 2. Hippocampal classifier evidence favors goal and sub-goal (intervening) locations over alternative locations. (**A**) "Future" classifier confusability during planning. Second to the true goal, the classifier most frequently guessed the sub-goal along the planned route (blue arrow). (**B**) Pairwise comparison of sub-goal versus alternative route evidence. Across trials, mean classifier evidence favors the sub-goal over the alternative locations. Error bars reflect the group SEM. ***$P < 0.001$.

A second central question is whether the human hippocampus not only supports prospective representation of goal states but also mediates route retrieval during planning. To the extent that planning navigational events incorporates replay of important locations along the route, classifier evidence should favor intervening sub-goals over other nongoal locations. Consistent with this prediction, during navigation planning, the location that was most confusable with the goal was the intervening sub-goal along the optimal route (Fig. 2A and supplementary materials). Direct comparisons of confusability of the goal with the sub-goal versus with the other nongoal locations revealed that the sub-goal was the most favored class (Fig. 2B and supplementary materials).

We also tested whether hippocampal prospective coding is accompanied by future goal–state evidence within a broader cortical network that is thought to subserve the representation and imagery of spatial context features. Specifically, the perirhinal cortex (PRC) may code for item content (environmental cue information) of goal locations (*36*), and the parahippocampal cortex (PHC) and RSC may support planning and future event simulation (*1*) through their putative roles in contextual reinstatement and location coding

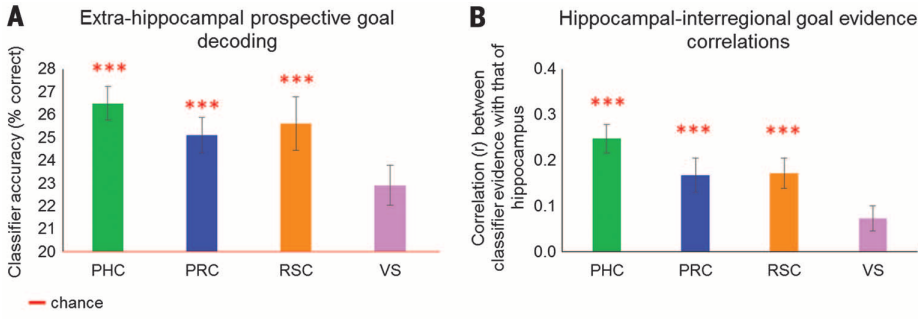

Fig. 3. Prospective evidence in extrahippocampal ROIs. (**A**) Future goal decoding during prospective planning. (**B**) Correlation (Pearson's *r*) between trial-by-trial evidence strength from the "future" classifier in the hippocampus and in extrahippocampal ROIs. Error bars reflect the group SEM. ***$P < 0.001$.

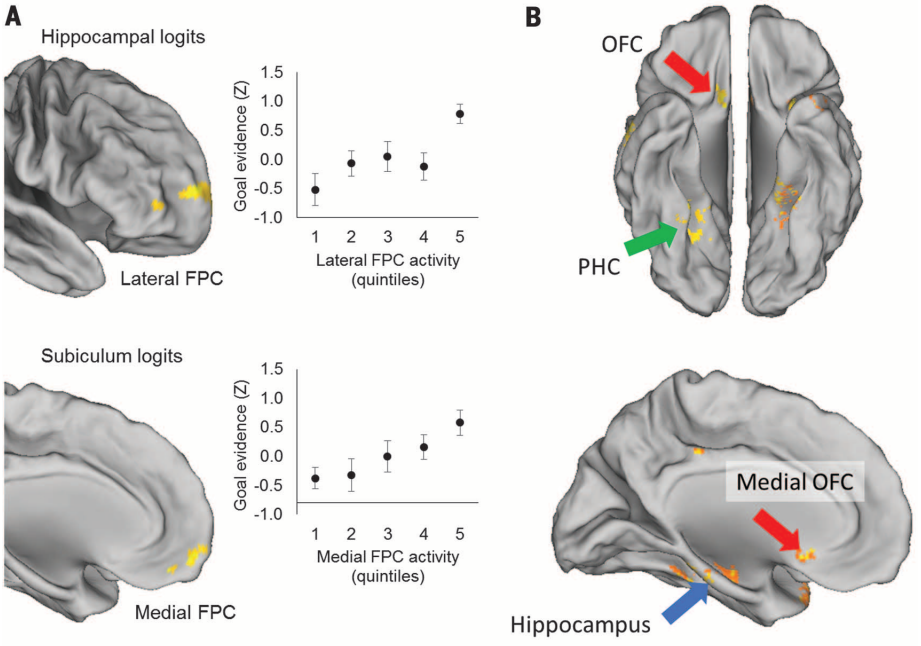

Fig. 4. Prefrontal cortical regions implicated in navigational planning. (**A**) The strength of prospective goal representation in the hippocampus (top) and subiculum (bottom) correlated with univariate activity in the FPC. Plots illustrate the underlying relationship between "future" classifier (goal) evidence (*Z*-score, logits) and the strength of FPC activity extracted from peak voxels. Error bars reflect the group SEM. (**B**) A whole-brain searchlight revealed goal decoding in a core network including the hippocampus, MTL cortex, and OFC. $P < 0.01$, voxel-wise threshold; cluster-corrected $P < 0.05$.

(*8*, *10*, *11*, *33*, *37*). Classification of planning period activity on the basis of the future goal was significantly above chance in each of these regions (Fig. 3A and supplementary materials). VS, which has been implicated in coding motivational signals in space (*19*), exhibited only marginally significant coding for future goal states. Among these a priori ROIs, a whole-brain searchlight revealed local patches in the hippocampus and PHC that exhibited significant goal coding (supplementary materials). Within our PHC, PRC, and RSC ROIs, trial-by-trial classifier evidence for the goal location positively correlated with that in the hippocampus (Fig. 3B and supplementary materials), supporting the hypothesis that their combined representational properties contribute to the multifeatural representation of future spatial contexts.

Top-down, controlled access to episode-specific details in the hippocampus is hypothesized to rely on hippocampal interactions with the PFC (*6*, *23*, *38*). Computations in the PFC may be important for both expressing goal-relevant mnemonic codes in the hippocampus and integrating hippocampal output into strategic planning. We tested this mechanistic framework by measuring functional connectivity between (i) the hippocampus (more broadly) and hippocampal subfields (more specifically) and (ii) PFC planning period univariate activity and "future" classifier evidence. Planning period activity in the lateral and medial frontopolar cortex (FPC), a region posited to enable prospective expression of memory and help integrate hippocampal output into route plans (*22*, *23*), significantly positively correlated with trial-by-trial "future" classifier evidence in the hippocampus and its subiculum subfield (Fig. 4A). Follow-up analysis of these regions revealed only modest "future" classification in the lateral FPC (that did not survive correction for multiple comparisons; supplementary materials). Instead, the whole-brain searchlight analysis (Fig. 4B) revealed significant "future" classification in the orbitofrontal cortex (OFC), which, critically, is known to connect to and functionally interact with the hippocampus during memory-guided navigation (*11*, *39*). (Methods and complete lists of significant clusters for these analyses are given in the supplementary materials.) Further supporting the importance of functional interaction between the PFC and hippocampal prospective codes in navigational planning, we observed a positive relationship between FPC and (at a modest level) OFC "future" classifier evidence and hippocampal "future" classifier evidence (supplementary materials). Together, these findings suggest that the OFC is part of a hippocampal network that codes for prospective goals and that the FPC plays a role in modulating hippocampal coding, providing cognitive control machinery through which route plans are formed and prospection is achieved (*22*, *23*).

To plan future behavior, humans and animals must be able to represent goals within an environment, as well as to retrieve potential means of reaching these goals. Our data indicate that the hippocampus, interacting with a functionally linked neocortical network (MTL cortex, RSC, and OFC), provides a mechanism for such mental simulation. In particular, our data encompass several important advances: We demonstrate that the human hippocampus contributes to goal-directed navigation, in part through representing future goal states as well as features of the current location (*32*), and, critically, we provide evidence that such prospective retrieval includes episodic simulation of the intended route. Although it remains to be seen whether similar coding and computations occur in more complex large-scale environments, such as those that humans traverse in daily life (*40*), this work bridges the prospective coding of navigational goals in the human hippocampus with related findings in rodents (*3*, *4*, *6*, *17*). Moreover, models of episodic memory and navigation (*6*, *23*, *38*) emphasize the importance of hippocampal-prefrontal interactions for representing navigational events and route planning. Our results provide evidence for an association between prospective hippocampal representations and putative planning processes in the FPC. More broadly, these findings illuminate the mechanistic role of the hippocampus, along with an extended MTL cortex, orbitofrontal, and retrosplenial network, in memory-guided simulation of future events (*1*, *2*). This network, along with the FPC, links look-ahead–like processes with goal-directed planning, which together enable humans to think prospectively.

REFERENCES AND NOTES

1. D. L. Schacter, D. R. Addis, *Philos. Trans. R. Soc. Lond. B Biol. Sci.* **364**, 1245–1253 (2009).
2. R. L. Buckner, D. C. Carroll, *Trends Cogn. Sci.* **11**, 49–57 (2007).
3. E. R. Wood, P. A. Dudchenko, R. J. Robitsek, H. Eichenbaum, *Neuron* **27**, 623–633 (2000).
4. I. Lee, A. L. Griffin, E. A. Zilli, H. Eichenbaum, M. E. Hasselmo, *Neuron* **51**, 639–650 (2006).
5. D. M. Smith, S. J. Mizumori, *J. Neurosci.* **26**, 3154–3163 (2006).
6. H. T. Ito, S.-J. Zhang, M. P. Witter, E. I. Moser, M.-B. Moser, *Nature* **522**, 50–55 (2015).
7. J. Ferbinteanu, M. L. Shapiro, *Neuron* **40**, 1227–1239 (2003).
8. T. I. Brown, M. E. Hasselmo, C. E. Stern, *Hippocampus* **24**, 819–839 (2014).
9. T. I. Brown, C. E. Stern, *Cereb. Cortex* **24**, 1906–1922 (2014).
10. T. I. Brown, R. S. Ross, J. B. Keller, M. E. Hasselmo, C. E. Stern, *J. Neurosci.* **30**, 7414–7422 (2010).
11. T. I. Brown, R. S. Ross, S. M. Tobyne, C. E. Stern, *Neuroimage* **60**, 1316–1330 (2012).
12. T. I. Brown, A. S. Whiteman, I. Aselcioglu, C. E. Stern, *J. Neurosci.* **34**, 2314–2320 (2014).
13. M. E. Hasselmo, H. Eichenbaum, *Neural Netw.* **18**, 1172–1190 (2005).
14. M. E. Hasselmo, *Neurobiol. Learn. Mem.* **92**, 559–573 (2009).
15. M. E. Hasselmo, C. E. Stern, *Neuroimage* **85**, 656–666 (2014).
16. A. Johnson, A. D. Redish, *J. Neurosci.* **27**, 12176–12189 (2007).
17. A. M. Wikenheiser, A. D. Redish, *Nat. Neurosci.* **18**, 289–294 (2015).
18. D. R. Addis, A. T. Wong, D. L. Schacter, *Neuropsychologia* **45**, 1363–1377 (2007).
19. M. A. A. van der Meer, A. Johnson, N. C. Schmitzer-Torbert, A. D. Redish, *Neuron* **67**, 25–32 (2010).
20. P. Byrne, S. Becker, N. Burgess, *Psychol. Rev.* **114**, 340–375 (2007).
21. N. Burgess, S. Becker, J. A. King, J. O'Keefe, *Philos. Trans. R. Soc. London B Biol. Sci.* **356**, 1493–1503 (2001).
22. N. Ramnani, A. M. Owen, *Nat. Rev. Neurosci.* **5**, 184–194 (2004).
23. H. J. Spiers, S. J. Gilbert, *Front. Hum. Neurosci.* **9**, 125 (2015).
24. J. F. Miller *et al.*, *Science* **342**, 1111–1114 (2013).
25. A. D. Ekstrom *et al.*, *Nature* **425**, 184–188 (2003).
26. L. R. Howard *et al.*, *Curr. Biol.* **24**, 1331–1340 (2014).
27. K. R. Sherrill *et al.*, *J. Neurosci.* **33**, 19304–19313 (2013).
28. H. J. Spiers, E. A. Maguire, *Hippocampus* **17**, 618–626 (2007).
29. C. F. Doeller, C. Barry, N. Burgess, *Nature* **463**, 657–661 (2010).
30. M. J. Chadwick, A. E. J. Jolly, D. P. Amos, D. Hassabis, H. J. Spiers, *Curr. Biol.* **25**, 87–92 (2015).
31. V. Sulpizio, G. Committeri, G. Galati, *Front. Hum. Neurosci.* **8**, 716 (2014).
32. D. Hassabis *et al.*, *Curr. Biol.* **19**, 546–554 (2009).
33. S. A. Marchette, L. K. Vass, J. Ryan, R. A. Epstein, *Nat. Neurosci.* **17**, 1598–1606 (2014).
34. S. A. Marchette, L. K. Vass, J. Ryan, R. A. Epstein, *J. Neurosci.* **35**, 14896–14908 (2015).
35. S. McKenzie, N. T. M. Robinson, L. Herrera, J. C. Churchill, H. Eichenbaum, *J. Neurosci.* **33**, 10243–10256 (2013).
36. J. C. Liang, A. D. Wagner, A. R. Preston, *Cereb. Cortex* **23**, 80–96 (2013).
37. E. M. Aminoff, K. Kveraga, M. Bar, *Trends Cogn. Sci.* **17**, 379–390 (2013).
38. R. Navawongse, H. Eichenbaum, *J. Neurosci.* **33**, 1002–1013 (2013).
39. H. Barbas, G. J. Blatt, *Hippocampus* **5**, 511–533 (1995).
40. T. Wolbers, J. M. Wiener, *Front. Hum. Neurosci.* **8**, 571 (2014).

ACKNOWLEDGMENTS

This work was supported by the National Institute of Mental Health (grant R01-MH076932) and the Wallenberg Network Initiative on Culture, Brain, and Learning. It was also made possible through the support of a grant from the John Templeton Foundation, "Prospective Psychology Stage 2: A Research Competition," to M. Seligman. The opinions expressed in this publication are those of the authors and do not necessarily reflect the views of the John Templeton Foundation. This work was additionally supported by fellowships from the NSF Graduate Research Fellowship Program, the NSF Integrative Graduate Education and Research Traineeship program, and the Natural Sciences and Engineering Research Council of Canada. Raw data are archived on the Stanford Neuroscience Institute server and will be made available upon request.

SUPPLEMENTARY MATERIALS

www.sciencemag.org/content/352/6291/1323/suppl/DC1
Materials and Methods
Supplementary Text
Figs. S1 to S6
References (*41*–*58*)

14 December 2015; accepted 12 May 2016
10.1126/science.aaf0784

NEURODEVELOPMENT

Oligodendrocyte heterogeneity in the mouse juvenile and adult central nervous system

Sueli Marques,[1]* Amit Zeisel,[1]* Simone Codeluppi,[1,2] David van Bruggen,[1] Ana Mendanha Falcão,[1] Lin Xiao,[3,4] Huiliang Li,[3] Martin Häring,[1] Hannah Hochgerner,[1] Roman A. Romanov,[1,5] Daniel Gyllborg,[1] Ana B. Muñoz-Manchado,[1] Gioele La Manno,[1] Peter Lönnerberg,[1] Elisa M. Floriddia,[1] Fatemah Rezayee,[1] Patrik Ernfors,[1] Ernest Arenas,[1] Jens Hjerling-Leffler,[1] Tibor Harkany,[1,5] William D. Richardson,[3] Sten Linnarsson,[1]† Gonçalo Castelo-Branco[1]†

Oligodendrocytes have been considered as a functionally homogeneous population in the central nervous system (CNS). We performed single-cell RNA sequencing on 5072 cells of the oligodendrocyte lineage from 10 regions of the mouse juvenile and adult CNS. Thirteen distinct populations were identified, 12 of which represent a continuum from *Pdgfra*$^+$ oligodendrocyte precursor cells (OPCs) to distinct mature oligodendrocytes. Initial stages of differentiation were similar across the juvenile CNS, whereas subsets of mature oligodendrocytes were enriched in specific regions in the adult brain. Newly formed oligodendrocytes were detected in the adult CNS and were responsive to complex motor learning. A second *Pdgfra*$^+$ population, distinct from OPCs, was found along vessels. Our study reveals the dynamics of oligodendrocyte differentiation and maturation, uncoupling them at a transcriptional level and highlighting oligodendrocyte heterogeneity in the CNS.

Oligodendrocytes ensheath axons in the central nervous system (CNS), allowing rapid saltatory conduction and providing metabolic support to neurons. Although a largely homogeneous oligodendrocyte population is thought to execute these functions throughout the CNS (*1*), these cells were originally described as morphologically heterogeneous (*2*). It is thus unclear whether oligodendrocytes become morphologically diversified during maturation through interactions within the local environment or whether there is intrinsic functional heterogeneity (*3*–*5*). We analyzed 5072 transcriptomes of single cells expressing markers from the oligodendrocyte lineage, isolated from 10 distinct regions of the anterior-posterior and dorsal-ventral axis of the mouse juvenile and adult CNS (Fig. 1, A and B). Biclustering analysis (*6*) (figs. S1B and S15), hierarchical clustering (Fig. 1C), and differential expression analysis (tables S1 and S2) led to the identification of 13 distinct cell populations. *t*-Distributed stochastic neighbor embedding (t-SNE) (Fig. 2A) supported by pseudotime analysis (fig. S2, A and B) indicated a narrow differentiation path connecting oligodendrocyte precursor cells (OPCs) and myelin-forming oligodendrocytes, which then diversify into six mature states.

Oligodendrocyte precursor cells coexpressed *Pdgfra* and *Cspg4* (Fig. 2B and figs. S1B and S10), and 10% coexpressed cell cycle genes (fig. S2, E and F), consistent with a cell division turnover of 19 days in the juvenile cortex (*7*). Several genes (such as *Fabp7* and *Tmem100*) identified in OPCs were previously associated with astrocytes and radial glia (*6*) (figs. S1B, S3, and S10), consistent with the origin of OPCs from radial glia–like cells, as well as their capacity to generate astrocytes in injury paradigms (*8*).

[1]Laboratory of Molecular Neurobiology, Department of Medical Biochemistry and Biophysics, Karolinska Institutet, SE-17177 Stockholm, Sweden. [2]Department of Physiology and Pharmacology, Karolinska Institutet, SE-17177 Stockholm, Sweden. [3]Wolfson Institute for Biomedical Research, University College London, Gower Street, London WC1E 6BT, UK. [4]Institute of Neuroscience, Second Military Medical University, 800 Xiangyin Road, Shanghai 200433, China. [5]Department of Molecular Neurosciences, Center for Brain Research, Medical University of Vienna, Vienna, Austria.
*These authors contributed equally to this work. †Corresponding author. Email: sten.linnarsson@ki.se (S.L.); goncalo.castelo-branco@ki.se (G.C.-B.)

Editor's Summary

Brain activity to represent the future

How do humans navigate from A to B? Brown *et al*. developed a virtual reality task to investigate the neural representations that support human navigational planning. Highly specific activity of the hippocampus and related brain areas represented the future locations to which participants eventually moved. Network-level interactions of the hippocampus with the prefrontal cortex thus enable flexible representation of planned destinations.

Science, this issue p. 1323

www.sciencemag.org/content/352/6291/1323/suppl/DC1

Supplementary Materials for

Prospective representation of navigational goals in the human hippocampus

Thackery I. Brown,* Valerie A. Carr, Karen F. LaRocque, Serra E. Favila, Alan M. Gordon, Ben Bowles, Jeremy N. Bailenson, Anthony D. Wagner*

*Corresponding author. Email: thackery@stanford.edu (T.I.B.); awagner@stanford.edu (A.D.W.)

Published 10 June 2016, *Science* **352**, 1323 (2016)
DOI: 10.1126/science.aaf0784

This PDF file includes:

Materials and Methods
Supplementary Text
Figs. S1 to S6
Full Reference List

Materials and Methods

Participants

Twenty right-handed healthy volunteers (9 female) with a mean age of 24.3yrs (range 20-34yrs) were recruited from Stanford University and the surrounding communities. All participants had normal or corrected-to-normal color vision. Two males and one female participant were excluded from the study at the end of Day 1 due to inability to learn the goal locations within the environment. Informed written consent was obtained from all participants, who were paid for their participation in a manner approved by the Stanford University Institutional Review Board. Payment was not conditioned on success.

Experimental design

Task stimuli consisted of a circular track in a virtual open-field environment, and 10 visually distinct color fractal images. The virtual environment and navigation task were presented using Vizard 3.0 (http://www.worldviz.com/products/vizard), a Python-based virtual reality development package. For each participant, five random pairings of the 10 fractals were randomly associated with five distinct goal locations along the circular track. The environment had no local landmarks, encouraging participants to rely on distal environmental cues to form spatial knowledge of the environment. Each goal location had an error radius of 10 virtual units from the location center; participants were required to navigate to within the correct approximate quintile during the scanned navigation task for the trial to be considered "correct". The circular track was 110 virtual units in circumference, and the goal locations were distributed around the track at coordinates jittered from a uniform distribution across participants within the constraint that their error radii did not overlap; this ensured that the fixed locations for each participant were not equidistant from each other. As such, jittering the positions in this manner encouraged participants to attend to the precise spatial location of the goals within the environment during training, since the visible fractals/goal centers were not equidistant in space or traversal time. Navigation speed was set at 20s to circumnavigate the track.

Day 1: Training task

Participants learned to navigate the environment approximately 24hrs prior to performing the cued navigation task in the scanner. The environment and goal locations were learned through trial and error, such that when errors were made on a training trial, participants received correctional feedback. Errors entailed taking a sub-optimal route (i.e., the longer direction) around the track, failing to accurately reach the correct goal, or both. Feedback was presented by letters overlaid on the screen communicating the nature of the error (e.g. "Correct location. Wrong direction") followed by computer-automated movement to the correct heading and position in the environment.

Training consisted of three stages. In total, participants performed 220 trials (60, 80, and 80 trials in each stage, respectively) that followed a similar structure to that of the scanning task (Fig. 1C). In all stages, participants were placed at a pseudorandom position in the environment, and their view panned to the ground where they saw one fractal cueing them to their current goal; they then selected a direction to navigate around the track, and then actively navigated to the goal location. For the first two stages of training, both fractals of each pair were visible at their respective goal locations as

participants navigated around the track. These stages of training enabled participants to learn the precise goal locations within the environment and the cue mappings to the locations.

During Stage 1, after being presented one fractal cue, the computer pseudorandomly selected a direction (clockwise or counter-clockwise) in which the participant would navigate for that trial. This ensured participants viewed each goal location from both directions during their initial exposure to the environment. During Stage 2, participants chose the direction that would enable them to reach the goal most efficiently. This training stage emphasized learning the spatial relationships between the precise goal locations in the environment. Stage 3 was identical to the Day 2 scanning task, meaning that the fractals were no longer visible at the goal locations during active navigation. Stage 3 reinforced spatial knowledge of the environment and localization of the now-hidden goal locations to the correct approximate quintiles on the basis of distal environmental cues. Stages 2-3 required memory-guided navigation to every goal from every other location, with navigation to a specific location/goal occurring via traversal of both directions an equal number of times. In order to participate in the Day 2 scanning session, participants had to master the task by the end of Stage 3 training, defined as navigating the correct direction to each correct location on all test trials (i.e., 100% accuracy).

Day 2: Scanning task

The scanning task was broken into 16 runs of 10 trials each, resulting in a total of 32 trials per goal location. Across all runs, participants navigated to every goal from every other location and traversed both directions to the goal an equal number of times. The design also balanced the intervening (sub-goal) locations for the subset of trials where participants were navigating to more distal goal locations. The timing of the scanning task was optimized for later pattern classification analysis: Each trial began with participants facing the ground (on the very first trial of a scanning run, participants first viewed their position and heading in the environment for 7s prior to their perspective panning toward the ground). A fractal cue was presented on the ground, with cue onset synchronized with the scanner TR. Cues were displayed for 2s, followed by a 7-9s delay during which the fractal was replaced by a fixation cross. This structure helped segregate the hemodynamic response of the critical cued planning period from that of the subsequent active navigation period. After 7s of the post-cue delay, arrows pointing forward and backward replaced the fixation cross, and participants had an additional 2s to indicate via a button box whether they wanted to continue forward or to navigate in the opposite direction to efficiently reach the goal. Once a direction was selected, the participant's view panned up (1s) and navigation began.

Critically, participants could not turn around once navigation began. This encouraged participants to actively prospect over their future navigation during the cued planning period. All participants reported using the cue to try to bring the goal to mind and think about where the goal was in relation to their current position. Participants made a button press indicating when they had reached their goal. Their view then panned down to the ground (1s), and they were held in place with a fixation cross for a post-arrival delay period of ~8s (7s + time needed to synchronize the next trial's onset with the TR). This structure helped segregate the hemodynamic response of the cued planning period

from that of the perception of/arrival at the goal on the preceding trial. For trials in which participants made a navigational error, text was displayed on the screen for 1s indicating the nature of their error (e.g. "Correct location, Wrong direction"), after which participants were teleported to the correct location with the correct heading direction. They were able to view their corrected location for 2s prior to their view panning to the ground for the post-arrival delay.

Critically, the task was structured such that participants viewed the ground during the cue period, navigated to each goal location from both directions around the track and from every other goal location, and were cued by both fractal cues for a given goal an equal number of times. This design helped ensure that successful fMRI multivariate classification of either the current location or the future goal was based on pattern information related to spatial context coding that generalized across different perceptual and navigational experiences.

MRI data acquisition

Scanning was conducted on a 3T scanner equipped with a 32-channel head coil at the Stanford University Center for Cognitive and Neurobiological Imaging. Whole-brain high-resolution ($1.6mm^3$) functional images were acquired using a 3-band multiplexed imaging protocol (*41*) with blipped-controlled aliasing to improve the signal-to-noise ratio (*42*). Functional images were acquired with an acceleration factor of 2, and had an acquisition matrix of 146 x 146, with 25 slices per band, an echo time of 30ms, a flip angle of 77°, and a repetition time (TR) of 2s. Functional image slices were aligned parallel to the long axis of hippocampus. A total of four dummy scans were completed before data acquisition began to allow for stabilization of the MR signal. For anatomical localization and cross-participant alignment, high-resolution ($0.9mm^3$), T1-weighted spoiled gradient recalled echo structural images were collected (matrix = 256 x 256, echo time = 2.78ms, flip angle = 12°, and TR = 7.24s). Visual stimuli were projected onto a screen and viewed through a mirror; navigation responses were collected using an MR-compatible button box.

fMRI data analyses

Imaging analyses were conducted using SPM8 (Wellcome Department of Cognitive Neurology, London, UK). All BOLD images were reoriented so the origin [i.e., coordinate xyz (0 0 0)] was at the anterior commissure. Motion correction was conducted by realigning the BOLD images to the first functional image acquired, and unwarping the BOLD images corrected for movement-by-susceptibility artifact interactions (*43*). High-resolution structural images were then coregistered with the mean BOLD images obtained during motion correction.

Principal analyses were conducted in single-subject native space, using manually defined anatomical regions of interest (ROIs). We delineated each participant's MTL subregions using established protocols (*44–49*), defining separate ROIs for hippocampus, entorhinal cortex (EC), perirhinal cortex (PRC), and parahippocampal cortex (PHC), and further subdividing hippocampus into subfields: CA1, a combined CA2/3/dentate gyrus subregion, and subiculum. We also defined anatomical ROIs within retrosplenial complex (RSC) and ventral striatum (VS), based on evidence that these regions may also contribute to prospection and navigational goal representation. RSC was defined based on

approximate functional localization of the human "retrosplenial complex" (e.g. *11*) – a functional region exhibiting orientation and location coding properties that may be analogous to those of retrosplenial cortex in rodents. RSC was defined by manually delineating a region on the dorsal bank of the parieto-occipital sulcus (POS), centered at the intersection of the calcarine sulcus with the POS and extending 7mm anterior and posterior to this point on each participant's anatomy. This approach resulted in a large anatomical region on the ventral anterior extent of medial parietal cortex (Fig. S3A) (note that this definition differs from a cytoarchitectonic delineation of Brodmann Areas 29/30). VS was manually defined based on anatomical guidelines for delineating the nucleus accumbens (*50*).

For group-level connectivity and searchlight analyses (see below), the coregistered high-resolution T1-weighted anatomical images were segmented into white and gray matter images and bias-corrected. The bias-corrected structural images and coregistered BOLD images were then spatially normalized into Montreal Neurological Institute (MNI) space using the Diffeomorphic Anatomical Registration using Exponentiated Lie algebra (DARTEL) algorithm (*51*) for accurate inter-subject registration. BOLD for the *hippocampal multivariate-univariate connectivity* (see below) were resampled during normalization to $2mm^3$ isotropic voxels and spatially smoothed using a 6mm full-width at half-maximum Gaussian kernel. Searchlight maps were not smoothed during normalization.

Data modeling

Our analyses targeted the ability to successfully categorize trial-specific fMRI patterns on the basis of *current* location and of *future*/prospective goal state. Consequently, we focused our multi-voxel pattern analyses (MVPA) on pattern information from the initial cue period of the task. To reduce the influence of interference from adjacent task components on identification of planning period pattern information, features were generated as single-trial parameter estimates using a GLM approach in SPM. Planning periods were modeled with multiple single-trial regressors in one GLM (2s duration, convolved with the canonical hemodynamic response function) to estimate voxel-level BOLD activity related to current position (*current* classifier) and to prospective goal (*future* classifier) during the rapid prospection that putatively occurred during initial planning (note that pattern information from subsequent planning periods in our task is separated by a substantial amount of time [>30s]). The remaining task components were modeled at the condition level (i.e., multiple trials per condition): (a) an arrow response regressor (stick function) modeled motor response events for selecting the direction around the track just prior to navigation; (b) five Navigation Phase regressors (variable duration epochs, based on path length) modeled activity during active navigation to each of the five respective goal locations; (c) five Goal Response regressors (stick function) modeled the motor response events terminating navigation; and (d) five Post-arrival Goal holding period regressors (7s) modeled delay period activity following successful navigation. Error trials, an 8s lead-in and lead-out period for each run, and the delay following the planning period cue were left unmodeled. The six motion parameters, computed during realignment were included in the models as regressors of non-interest.

Rodent and theoretical models of episodic memory and navigation (*6*, *23*, *38*) emphasize the importance of hippocampal-prefrontal interactions for representing

navigational events and route planning. To test whether prefrontal activation co-varies with prospective coding in hippocampus, we also conducted a *hippocampal multivariate-univariate connectivity* analysis. We used the same modeling approach described above, but collapsed the single-trial cue events into one regressor, and paired it with a parametric modulator of trial-by-trial hippocampal *future* classifier evidence for the goal. To obtain a continuous measure of evidence strength, we leveraged the logit (log odds) of the trial-wise probabilistic classifier output for the target class (goal location). This allowed us to quantify how fluctuation in the trial-by-trial strength of hippocampal goal representations during initial planning co-varies with univariate activity elsewhere in the brain.

Principal ROI classification analyses

The principal classification analyses were conducted using ROI-specific single-trial parameter estimates (betas) from the planning period as features. Data preprocessing for classification was performed using the Princeton MVPA Toolbox (http://www.pni.princeton.edu/mvpa/) and custom Matlab scripts. Signal in each voxel was *Z*-scored across trials within-session prior to classification; for single-trial beta classification, no additional preprocessing was conducted. Standard multi-class one-vs-the-rest classification was performed using a logistic regression classifier with L2 regression regularization (penalization parameter = 1 for all classifications), as instantiated in the LIBLINEAR classification library (http://www.csie.ntu.edu.tw/~cjlin/liblinear/). A fixed penalty of 1 was used for consistency in classifier parameters across participants and across iterations within each participant. Note that a penalty of 1 was frequently selected when employing an automated non-peaking penalty optimization approach in a subset of participants; this approach was not adopted, because it would result in inconsistent regularization across trials and participants.

Principal classification analyses were conducted with two separate classifiers: one targeting current location coding (*current* classifier) and the other targeting prospective goal coding (*future* classifier). The same planning period data were submitted to both classifiers, but the location labels for the trials (*current* or *future* location) differed. Both classification analyses were accomplished by 16-fold cross validation in which one run was left out for testing on each fold. Within each cross-validation fold, 200 balancing iterations were run, such that the training data were repeatedly subsampled prior to a given training-testing iteration. The number of training trials included in each balancing iteration varied across cross-validation folds and was chosen as the maximum number of trials that allowed for equal numbers of trials for each goal location, start location, and cue image in the training set in a manner that ensured the maximum number of trials in the training set with equal numbers of trials for each goal location, start location, and cue image in the training set. Five-way classifier performance was measured using 2-tailed paired-sample *t*-tests against empirically derived chance, established within each participant by pseudorandomly shuffling the class labels (preserving the same number of trials per condition per scan session, and ensuring that trials corresponding to the same location could not be adjacent in time, consistent with the true task structure) over 200 balanced iterations per cross-validation fold, and calculating the resulting mean classification accuracy from this distribution (group chance means from 5-goal *future* and *current* classifiers: hippocampus *future*, *current* = 20.7%, 20.1%; PHC *future*, *current* =

20.2%, 19.9%; PRC *future*, *current* = 20.2%, 20.1%; RSC *future*, *current* = 19.8%, 20.0%; VS *future*, *current* = 20.3%, 20.3%). The balanced cross-validation folds were nested within each label shuffling.

Recent evidence from related tasks in rodents suggests functional specialization within rodent hippocampus, with the CA1 subfield carrying more reliable episode-specific route coding (*6*) than CA3. Moreover, computational models propose that large place cell firing fields (*52*) centered over goal locations in the subiculum – a major output region of hippocampus – could give rise to goal-coding signals (*53*). Accordingly, in addition to quantifying evidence for future goal states across the whole hippocampus, we explored possible analogous subfield differentiation in humans by running our classification analyses separately within anatomically defined CA1, CA2/3/DG, and subiculum subfields.

Another key goal of our experiment was to test whether hippocampal prospective coding is accompanied by goal state evidence within a broader hippocampal network (including MTL cortex, RSC, and VS) whose anatomical interconnectivity could subserve representation and imagery of features of the desired location (Fig. S3A). Accordingly, we examined *current* location and *future* goal decoding using MVPA on BOLD data within these regions. We further examined the correlations between trial-by-trial classifier evidence in these areas and that within hippocampus. This latter analysis, termed "representational connectivity", provides an index of the relationship between the strength of goal-related codes within hippocampus and these targeted areas (Fig. 3B), with more positive correlations suggestive of tighter coupling between goal representations in these regions. Note: for these and all other correlation analyses, individual participant *r* values were submitted to a Fisher *z*-transformation prior to computing statistical significance.

Intra-hippocampal and whole-brain searchlight analyses

To further characterize the spatial distribution of neural patterns coding for current and future locations within hippocampus and throughout the brain, we complemented our principal ROI-level analyses with two searchlight classification analyses that assessed local decoding accuracies (*54*). The searchlight analysis has the added benefit of controlling for the number of voxels examined across regions during classification – which inherently vary in anatomically defined ROIs (mean number of voxels ± SEM: hippocampus = 2103±76, PHC = 1670±132, PRC = 1313±127, RSC = 1708±77, VS = 411±29). We addressed three questions of interest: 1) Is there a spatial distribution of location coding along the rostro-caudal axis of hippocampus? 2) Do prefrontal regions also carry representational information related to the future goal? (3) Is decoding of future spatial contexts anatomically selective or is it ubiquitous, being observed throughout the brain?

We addressed these questions using (a) a searchlight analysis anatomically restricted to each participant's hippocampus, with the outcomes submitted to a mixed-effects analysis treating participant as a random effect, and (b) a whole-brain searchlight restricted to each participant's gray-matter volume derived from SPM, with the outcomes again submitted to mixed-effects analysis. In both cases, we performed the *current* and *future* location classifications as described above, using the single-trial parameter estimates and the same classifier parameters as in the ROI analyses, with the key

difference being that classification was performed on local spherical masks centered individually on every voxel in the gray-matter search volume. Each spherical mask had a fixed radius of 3 voxels (note: individual voxels were excluded when they extended beyond the search volume). Individual participant searchlight classification accuracy maps were then normalized to MNI space using DARTEL (preserving the native 1.6mm^3 resolution, and without additional smoothing), and submitted to group-level significance testing in the same manner as the *hippocampal multivariate-univariate connectivity* analysis described below. We applied cluster-extent thresholds (k) of 15 and 60 voxels to the high-resolution hippocampal and whole-brain searchlights, respectively, to maintain a familywise error rate of $p < 0.05$ given a voxel-level threshold of $p < 0.01$. Classifier significance was computed against mean baseline searchlight maps generated from shuffling the class labels 200 times, and, for each shuffled label set, performing classification over 10 balancing iterations (of the training set labels) per cross-validation fold. A complete searchlight accuracy map was generated for a given shuffled label set and balancing iteration, preserving the inherent dependence across searchlights, and the mean baseline map was generated after all iterations had run.

Supplementary text

Behavioral performance

Participants performed the scanning-phase virtual navigation task (Day 2) with a high degree of accuracy, correctly selecting the optimal route and successfully localizing the goal location within the error radius on 94.4% of trials (SEM ±1.75). Accuracy was high for all goal locations (Fig. S1A) and did not differ by location (repeated-measures ANOVA: $F_{(2.29,36.7*)} = 1.17$; $p = 0.33$ [*Huynh-Feldt corrected for non-sphericity]). Participants selected the navigational direction at the end of the planning period delay within a mean of 605ms (SEM ±28.9ms); this reaction time (RT) did not differ between locations (repeated-measures ANOVA: $F_{(4,64)} = 0.93$; $p = 0.45$) (Fig. S1B). For successful navigation trials, participants localized the goal locations with a high degree of precision, stopping within a mean of 3.94 virtual units (SEM: 0.18 units) of the center of error radius. Again, goal precision did not differ between locations (repeated-measures GLM: $F_{(4,64)} = 0.43$; $p = 0.79$) (Fig. S1C). The group precision distribution across trials is visualized in Fig. S1D; notably, the mean level of precision reflects a very small perceptual change in distal location cues (Fig. S1E).

ROI-based current location and future goal location classification

We first trained and tested a *current* classifier on the basis of current (start) location during the planning period. As reported in the main text, classification was above chance in hippocampus (29.9%; the mean confusability is plotted in Fig. S2A,B), replicating and extending prior evidence for a current location code in human hippocampus (*32*, *55*) in the context of carefully controlled perceptual input. We also observed a modest tendency towards above chance classification in the broader network of *a priori* targeted anatomical ROIs (MTL cortex, RSC, and VS) (Fig. S3A): PHC (22.8%, $t_{(16)} = 2.52$, $p = 0.02$), PRC (21.5%, $t_{(16)} = 1.26$, $p = 0.23$), RSC (23.8%, $t_{(16)} = 2.72$, $p = 0.02$) and VS (21.9%, $t_{(16)} = 2.90$, $p = 0.01$). While PHC, RSC, and VS had individually above-chance classification, classifier performance did not survive bonferroni correction for multiple comparisons (Fig. S3B).

Turning to our primary analyses, hippocampal classification on the basis of *future* location was significantly above chance (29.4%), as reported in the main text. Classifier evidence did not differ between the five goal locations (evaluated within each participant using 1-way ANOVAs of trial-by-trial evidence as a function of location: mean within-subject $F = 1.40$; mean $p = 0.45$; the mean confusion matrix is plotted in Fig. S2C), nor did hippocampal univariate signal (1-way ANOVA of mean parameter estimates for each trial as a function of location: mean within-subject $F = 0.99$; mean $p = 0.51$). The latter observation indicates that the five goals were not distinguished by coarse univariate activation differences. Across all trials, there was comparable confusability for locations proximal-to and distal-from the goal (Fig. S2D) (computed as mean confusability for all non-start, non-goal locations adjacent to or one location away from the goal; paired-sample *t*-test between proximal and distal confusability: $t_{(16)} = 0.12$; $p = 0.90$) [but see *Intervening sub-goal location decoding* below]. Confusability for the proximal (paired-sample *t*-test: $t_{(16)} = 1.85$; $p = 0.08$) and distal (paired-sample *t*-test: $t_{(16)} = 1.14$; $p = 0.27$) locations was not significantly greater than that of the start location.

Interestingly, while *current* location classification was significantly above chance in hippocampus, the *future* goal classifier exhibited little confusability with start location (Fig. S2C), and trial-by-trial *future* classifier evidence was uncorrelated with that of the *current* classifier (mean $r = -0.004$, one-sample *t*-test against zero: $t_{(16)} = -0.18$, $p = 0.86$). That is, greater evidence for the start does not predict greater evidence for the goal. These results are consistent with neural codes for both current and future states being expressed during planning (within the temporal resolution afforded by fMRI), with stronger representation of start location not reliably predicting stronger reinstatement of the future goal location.

Within the hippocampal subfields, we observed comparable classification in subiculum (26.5%, SEM 0.95), CA1 (25.2%, SEM 0.96), and CA2/3/DG (24.5%, SEM 1.05), such that there were no significant differences between regions (repeated-measures ANOVA $F_{(2,32)} = 0.85$; $p = 0.44$).

As reported in the main text, within our broader network of *a priori* targeted anatomical ROIs (MTL cortex, RSC, and VS), *future* goal classification was above chance, bonferroni corrected for multiple comparisons, in PHC (26.5%, $t_{(16)} = 7.45$, $p = 1.38\text{x}10^{-6}$), PRC (25.1%, $t_{(16)} = 5.28$, $p = 7.47\text{x}10^{-5}$), and RSC (25.6%, $t_{(16)} = 3.94$, $p = 0.001$); while classification was also individually above chance in VS (22.9%, $t_{(16)} = 2.17$, $p = 0.05$), it did not survive correction for multiple comparisons. Moreover, trial-by-trial evidence for the goal in these regions significantly correlated with that in hippocampus (PHC: mean $r = 0.25$, $t_{(16)} = 8.01$, $p = 5.50\text{x}10^{-7}$; PRC: mean $r = 0.17$, $t_{(16)} = 4.54$, $p = 3.35\text{x}10^{-4}$; RSC: mean $r = 0.17$, $t_{(16)} = 5.24$, $p = 8.09\text{x}10^{-5}$; VS: mean $r = 0.07$, $t_{(16)} = 2.59$, $p = 0.02$ [VS not significant after bonferroni correction for multiple comparisons]). A repeated-measures ANOVA revealed a marginal, non-significant effect of *future* versus *current* classifier performance across the hippocampal and extra-hippocampal ROIs ($F_{(1,64)} = 2.40$; $p = 0.06$), and no interaction between prospection (*future* vs *current* classifier) and location ($F_{(4,64)} = 1.38$; $p = 0.25$).

Cross-cue classification and evidence for goal reinstatement in hippocampus

Our future goal classification analysis approach required the classifier to identify pattern information consistent across navigational events (including different start/current

locations, different cues, and different traversal directions). To further confirm that prospective goal-related coding in hippocampus generalizes across cues, a new classifier was trained on planning period patterns from trials corresponding to only one of the cues for each goal, and tested on planning period patterns from trials corresponding to the other cue. The classifier was run across 200 iterations to equate trial numbers and to permute over cue/goal pairings in the training set. This is a challenging classification problem given that a) future goal and cue identity were intentionally perfectly correlated in the training set such that the classifier was free to learn features characteristic of either information type, and b) the training set was approximately halved in size relative to our main analysis (note that halving the trial count in the main *future* classifier analysis yielded attenuated classification of 26.3%). Importantly, while numerically lower, we observed significant above chance future goal classifier performance when training on the data with *one of the cues* for each goal and testing on the data with *the other cue* for each goal (24.6%; $t_{(16)} = 3.53$, $p = 0.003$). This outcome provides additional evidence that prospective spatial coding is a feature of human hippocampus.

Our principal cross-validated MVPA analyses provide a perceptually controlled evaluation of prospective event coding on the basis of future goal. We also sought to determine the degree to which features present upon goal arrival are reinstated during the initial planning period. That is, we quantified the degree to which pattern information during initial planning that codes for goal state is similar to the pattern information that is present upon goal arrival. For this analysis, we generated a novel set of single-trial parameter estimates from post-arrival goal periods in our original model. We then used the future classifier that was trained on planning period activity, testing the classifier on goal period patterns. Above chance classifier performance (26.8%; $t_{(16)} = 7.65$, $p = 1.00\text{x}10^{-6}$) on the testing set demonstrated that the features diagnostic of goal state during initial planning were present upon subsequent goal arrival, consistent with the representation of the experience at the goal being reinstated during planning. Importantly, this was the case even though one of the two cues was presented to participants during the planning period, but neither cue/fractal was present when participants arrived at the goal. This observation further argues that prospective goal coding in hippocampus extends beyond representing the fractal cue(s) associated with the goal. On this point, we also note that the ability to classify current location, which was associated with an entirely distinct set of fractals from the cue for the goal, further supports the presence of spatial context coding that extends beyond simple cue information.

Is there location clustering within human hippocampus?

Is successful location decoding in hippocampus based on (a) large-scale preference maps – with different locations predominantly driving spatially clustered populations of hippocampal voxels – or (b) more interleaved, distributed representations? To address this question, we conducted a "location clustering" analysis that leveraged the univariate data to quantify whether voxels with the same goal-location preference are spatially clustered beyond what would be expected given the inherent smoothness of our fMRI data. In this analysis, we first generated univariate preference maps (S4B-D), in which we computed the mean planning period parameter estimate for each goal location, and coded each hippocampal voxel's preferred location based on the maximum of these mean

parameter estimates. Visual examination of these preference maps suggests a highly interleaved, distributed pattern of location preference across voxels.

Next, we quantified the spatial clustering of location preference in these hippocampal maps. (1) First, we computed the modal preferred class in the voxels surrounding (but excluding) each center voxel (a local sphere). (2) Then we assigned a binary code to the center voxel of 1 or 0 (I_i), depending on whether the modal preference of the surrounding voxels matched that of the center voxel (i.e., is the preference of the center voxel successfully predicted by its surrounding voxels?). (3) Then we computed a clustering weight (W_i) for each local sphere as the number of voxels (excluding the center) with the modal preference, divided by the total number of voxels in the sphere. This provided a means of weighting the contribution of each individual voxel to the overall clustering score by the degree to which its surrounding voxels yielded a strong prediction about its preference. (4) Finally, we computed the overall clustering score for hippocampus from these searchlight statistics:

$$Clustering\ score = \sum (W_i \times I_i) \div \sum W_i$$

Thus, the hippocampal clustering score was a weighted mean, representing the degree to which location preferences across voxels are predicted by their neighbors, adjusted for the overall degree of shared location preference amongst the surrounding voxels in each searchlight.

Critically, we computed the clustering score for three different searchlight radii (one voxel, two voxels, and three voxels), to characterize the spatial extent of clustering in the data (since immediately adjacent voxels are expected to have a greater degree of shared signal due to the inherent smoothness in the data). In an initial analysis, each searchlight radius excluded the voxels that would be included in the next-smaller searchlight, such that the voxels submitted to the clustering analysis represented a "shell" of radius r surrounding the center voxel. By not re-sampling the same voxels with each increase in searchlight radius, this approach examined the degree to which voxels at a given radius predict the preference of the center voxel.

Due to inherent smoothness in BOLD data, some degree of clustering in "location preference" is expected independent of local representational properties. Therefore, significant clustering in hippocampus was determined by comparing true clustering scores of each participant against an empirically established baseline. The baseline was determined by scrambling class (goal location) labels for planning period parameter estimates and re-computing the clustering score for hippocampus. The scrambling preserved structural properties of the task (i.e., the same number of trials per condition per scan session, and trials corresponding to the same location could not be adjacent in time). Over 100 scrambling iterations, this approach allowed us to establish the degree of inherent clustering in the data due to its smoothness, independent of the true location preference information in the data.

Results of the "shell" clustering analysis (Fig. S4A) demonstrated that location clustering did not exceed that expected from inherent smoothness in the data: Across the three searchlight radii, a repeated-measures ANOVA revealed no main effect of *True* versus *Baseline* clustering ($F_{(1,16)} = 1.32$, $p = 0.27$). In addition, there was no interaction between *True* versus *Baseline* clustering and searchlight radius ($F_{(2,32)} = 1.57$, $p = 0.22$).

Finally, there was a main effect of searchlight radius ($F_{(2,32)} = 300.60$, $p = 2.00\text{x}10^{-16}$), reflecting a sharp drop in shared location preference with the center voxel from the immediately adjacent to more distal voxels. Note that, as this effect did not interact with *True* versus *Baseline* status, it reflects the inherent smoothness of the data rather than a change in location clustering across spatial extents. Paired-sample *t*-tests demonstrated that there was no difference ($t_{(16)} = -1.06$, $p = 0.305$) in True versus Baseline clustering even in voxels immediately adjacent to the center (radius = 1). It is possible that the preceding analysis failed to detect clustering because we used integrated across too few voxels, and thus had low sensitivity. To further explore possible clustering, we used volumes volumes (rather than shells) of radii 1, 2, and 3. Notably, we were similarly unable to predict a voxel's preference using volumes, as there was no main effect of True versus Baseline clustering ($F_{(1,16)} = 1.99$, $p = 0.18$); no interaction between True versus Baseline clustering and searchlight radius ($F_{(2,32)} = 1.97$, $p = 0.16$); and there was a significant main effect of searchlight radius ($F_{(2,32)} = 347.30$, $p = 2.00\text{x}10^{-16}$). Together, the lack of significant clustering above that expected in empirically established baseline data suggest that the representation of locations in our task is not reflected in large-scale preference maps in hippocampus (at the resolution afforded by fMRI).

Intervening sub-goal location decoding

To examine the extent to which reinstating representations of future locations during planning incorporates replay of significant locations along the intended route, we further considered planning period *future* classifier confusability as a function of the intervening sub-goal location along the planned route. For this analysis, the classifier was trained on the full dataset, but performance data were derived from the 50% of navigation trials in which participants navigated to a more distal (as opposed to adjacent) goal location – that is, trials on which one of the other possible locations lay along the future route between the start location and the end goal. As reported in the main text, overall classifier confusability was qualitatively greatest for these sub-goal locations (Fig. 2A). We computed the proportion of trials in which classifier evidence favored choosing the sub-goal over all other non-goal locations (regardless of whether the true goal had the highest evidence). A one-sample *t*-test against chance (25% in this four-location comparison) revealed that sub-goal locations were significantly favored over all other non-goal locations 28.7% (SEM = 1.36) of the time ($t_{(16)} = 2.69$, $p = 0.017$). We did not find significant evidence for the sub-goal in extra-hippocampal targeted ROIs (PHC: 25.3%, $t_{(16)} = 0.146$, $p = 0.886$; PRC: 27.1%, $t_{(16)} = 1.367$, $p = 0.193$; RSC: 26.9%, $t_{(16)} = 1.546$, $p = 0.144$; VS: 27.3%, $t_{(16)} = 1.768$, $p = 0.105$). Given significant sub-goal evidence in hippocampus, we also separately compared the mean rate at which classifier evidence favored the sub-goal vs. each of the other non-goal locations, again regardless of whether evidence for the goal state was greatest. Critically, the sub-goal had significantly greater evidence (i.e., higher confusability) relative to each of the other three locations (vs start: $t_{(16)} = 6.85$, $p = 5.45\text{x}10^{-6}$; vs alternate route location 1: $t_{(16)} = 4.21$, $p = 7.62\text{x}10^{-4}$; vs alternate route location 2: $t_{(16)} = 5.09$, $p = 1.33\text{x}10^{-4}$) (Fig. 2B).

We then quantified the relationship between goal and sub-goal evidence. We hypothesized that prospection over the goal would predict replay of the sub-goal. This is a challenging classification question to address, because there is a bias towards a negative relationship between goal and sub-goal evidence driven by the inherent interdependence

of the probabilistic evidence scores for each of the five locations. To control for this source of bias, we computed whether trial-by-trial evidence scores for the goal and sub-goal were less negatively correlated than expected by the inherent interdependence in the data. A null distribution for the correlation between the goal and sub-goal evidence scores was generated through a permutation analysis in which the sub-goal and alternate route location labels across trials were randomly shuffled over 1000 iterations. For each shuffling iteration the goal and shuffled "sub-goal" label evidence correlations were recomputed. Trial-by-trial evidence for the goal and the sub-goal showed a trend towards a more positive correlation than expected by inherent interdependence in the data (mean $r_{observed}$ *minus* r_{null} = 0.06, paired-sample *t*-test against null $t_{(16)} = 1.73$, $p = 0.10$), providing modest evidence that retrieval of one state predicted that of the other.

Finally, we conducted an exploratory analysis to examine whether there was evidence for temporal structure during the representation of the sub-goal and goal within hippocampus. While prospective hippocampal replay events happen in a temporally compressed manner in rodents, to the extent that our participants engaged in deliberate sequential retrieval during planning, the time-course of evoked BOLD patterns may reveal temporal differences in the relative strength of sub-goal and goal representations. To test this possibility, we conducted a leave-one-out cross-validation classification in which the classifier was trained and tested on the basis of future goal location, but using the motion-corrected BOLD time-course data (as opposed to single-trial parameter estimates). We observed minimal classification at the level of individual TRs; however, averaging BOLD patterns from adjacent time-points to improve temporal signal-to-noise-ratio improved our sensitivity to detect representational content. We compared classification for patterns generated from the weighted means of TRs 1-2 and 3-4 with weighting of 0.25-0.75 and 0.75-0.25, respectively. This weighting scheme was selected to emphasize pattern information centered over 2-4 and 4-6s, which corresponds to the rise and peak of hippocampal univariate time-course signal (Fig. S5A). Signal in each voxel was *Z*-scored across trials within-session prior to classification.

To partially account for the fact that sub-goal confusability may decrease as evidence for the goal increases from the first to the second TR bin, rendering estimation of the relative evidence between the two challenging, we computed classifier accuracy as the proportion of trials for which the sub-goal and goal had, separately, the highest confusability when compared to all other non-goal locations (i.e., start and alternate route locations 1 and 2) for the two TR bins. A repeated-measures ANOVA revealed a trend for an interaction ($F_{(1,16)} = 3.58$, $p = 0.08$) between location (sub-goal and goal) and time (TR bin). Direct comparison of the two locations revealed that the sub-goal was more confusable, relative to other non-goal locations, than the goal during the first TR bin ($t_{(16)} = 2.64$; $p = 0.02$) (Fig. S5B). While interpretative caution is clearly warranted, these findings suggest a trend towards sub-goal evidence manifesting sooner than goal evidence during planning.

Hippocampal multivariate-univariate connectivity

We leveraged the whole-brain data to test whether the strength of prospective goal representations in hippocampus and its subfields relates to univariate activity in prefrontal cortex. For this analysis, we analyzed prefrontal activity using smoothed, DARTEL-normalized functional data, with the strength of *future* classifier goal pattern

evidence (classifier logits) as a parametric modulator (as described above). Thus, for each participant, we estimated how trial-by-trial classifier evidence for goal state relates to univariate prefrontal activity. Resulting parametric modulator beta maps were entered into a second-level one-sample *t*-test in SPM8, treating participant as a random factor. The resulting group-level connectivity maps (Fig. 4A-B) were analyzed with a voxelwise statistical threshold of $p < 0.01$. Because of our strong prediction that prospective retrieval in our task is supported via hippocampal interactions with prefrontal regions, we conducted this connectivity analysis in a restricted region of interest volume composed of medial, orbital, and lateral prefrontal cortices (reducing the multiple-comparisons problem). The search volume was created by combining relevant AAL structural delineations (*56*) from the Wake Forest University (WFU) PickAtlas for SPM (*57*, *58*), and manually trimming the resulting mask to ensure targeted anatomical specificity. To limit the occurrence of spurious clusters, we applied a cluster-extent threshold (k) of 156 to maintain a family-wise error rate of $p < 0.05$, calculated using a 10,000 simulation Monte Carlo analysis in 3dClustSim (from the AFNI software package; http://afni.nimh.nih.gov/afni/). Importantly, adopting a cluster-level (rather than voxel-level) approach to correcting for multiple comparisons addresses the spatially continuous nature of the data. However, because the statistics are corrected at the cluster level, the data should be interpreted as revealing the presence of significant effects within the discrete clusters identified, and not that the amplitude of all voxels within each cluster would independently reach corrected significance.

As reported in the main text, activity in both lateral FPC ($t = 4.71$; xyz = 20, 68, 10) and medial FPC ($t = 4.65$; xyz = -2, 56, -10) was positively related to *future* classifier goal evidence (Fig. 4A-B). Within hippocampal subfields, only the representational strength in subiculum had significant above-threshold prefrontal connectivity. There were no significant pairwise differences between subfields when applying cluster correction. There were no significant differences between subicular and whole-hippocampus connectivity, and their patterns of functional connectivity overlapped at reduced voxelwise thresholds.

To illustrate the mean within-subject relationship between hippocampal/subicular classifier evidence and prefrontal activity, we extracted single-trial parameter estimates from peak lateral and medial FPC voxels for each participant, and plotted hippocampal/subicular classifier evidence against activity (Fig. 4A-B plots). Given the "causal" relationship between prefrontal computations and hippocampal coding suggested by rodent data (*6*, *38*), we plotted classifier evidence (y-axis) against prefrontal activity on the x-axis. To better illustrate the within-subject relationship between activity and evidence, evidence was binned by FPC activity quintiles for each participant, and quintile mean evidence strengths were *Z*-scored within-subject prior to plotting. Note that we cannot infer causality from our data, and these plots are included solely to illustrate the approximate relationship between classifier evidence and FPC univariate activity.

Searchlight decoding within hippocampus and whole-brain

A hippocampus-specific searchlight analysis revealed that local decoding within hippocampus was present in the hippocampal body, extending into the head (Fig. S6A) for both the *current* (Right $t = 6.34$; xyz = 30, -21, -18) and *future* (Left/Right $t = 4.87/4.73$; xyz = -29, -19, -16 / 32, -26, -13) classifiers. Of note, *current* classifier

decoding was only significant in the right hemisphere, even at a reduced voxel-level threshold of $p < 0.05$. However, submitting the *current* and *future* classifier searchlight accuracy maps to a pattern similarity analysis at the individual participant level (correlation between *current* and *future* classifier maps in vector form) revealed that the pattern of classifier accuracy within hippocampus was highly similar across current and future location decoding (Fig. S6B; mean $r = 0.739$; current classifier maps were more similar to future classifier maps than their empirical baseline maps: paired-sample t test: $t_{(16)} = 6.38$, $p = 9.00\text{x}10^{-6}$).

A whole-brain searchlight analysis further confirmed significant decoding of future goal location in hippocampus (Left $t = 4.31$; xyz = -27, -16, -19) and PHC (Left/Right $t = 6.01/5.89$; xyz = -27, -35, -18 / 19, -46, -11), and revealed additional effects in posterior OFC ($\text{Left}_{[\text{medial wall}]}/\text{Right}_{[\text{orbital surface}]}$ $t = 5.91/5.70$; xyz = -5, 16, -11 / 10, 16, -22), anterior insula (Left/Right $t = 6.90/5.87$; xyz = -27, 11, -14 / 38, 2, 3), and posterior cingulate cortex (Left $t = 5.08$; xyz = -2, -30, 40) (Fig. 4B). Consistent with the pattern of non-significant current location decoding from our ROI-based analyses, the *current* classifier whole-brain searchlight revealed that current location could not be decoded outside the hippocampus.

PFC goal coding and representational connectivity

Given the hypothesized role of PFC in guiding hippocampal memory-dependent planning, we conducted follow-up analyses using the PFC clusters identified in the *hippocampal multivariate-univariate connectivity* and *whole-brain searchlight* analyses. First, we examined whether FPC clusters identified in the *hippocampal multivariate-univariate connectivity*, while not exhibiting significant *future* classification at the whole-brain searchlight level, contained evidence coding for future goal location. Lateral and medial FPC cluster ROIs submitted to the *future* classifier exhibited low classification accuracy; these effects did not survive correction for multiple comparisons (mean *future* classifier accuracy: medial FPC cluster = 22%, $t_{(16)} = 1.72$, $p = 0.11$; lateral FPC = 22%, $t_{(16)} = 2.27$, $p = 0.04$).

Motivated by significant classification of future goal location in OFC, and weak evidence for classification of future goal location in FPC, we then examined whether these regions exhibited "representational connectivity" with hippocampus. *Future* classifier evidence in the right OFC searchlight cluster exhibited a modest positive correlation at the group level with that of hippocampus (mean $r = 0.05$, $t_{(16)} = 2.14$, $p = 0.05$). Correlations between the medial OFC searchlight cluster and hippocampus were not significant (mean $r = 0.04$, $t_{(16)} = 1.71$, $p = 0.11$). Given the uncorrected, modest significance, interpretative caution is warranted.

Paralleling the results of the *hippocampal multivariate-univariate connectivity* analyses, trial-by-trial evidence scores in medial and lateral FPC were positively correlated at the group level with those of the hippocampus and subiculum (medial FPC with hippocampus: mean $r = 0.08$, $t_{(16)} = 3.54$, $p = 0.003$; lateral FPC with hippocampus: mean $r = 0.07$, $t_{(16)} = 3.65$, $p = 0.002$; medial FPC with subiculum: mean $r = 0.07$, $t_{(16)} = 4.72$, $p = 2.31\text{x}10^{-4}$; lateral FPC with subiculum: mean $r = 0.05$, $t_{(16)} = 3.18$, $p = 0.006$). Importantly, these results suggest that while evidence for goal state in FPC is weak, goal-related evidence that *is* present is functionally linked with hippocampal evidence. Finally, evidence scores in medial FPC also significantly correlated with those in medial OFC

(mean $r = 0.06$, $t_{(16)} = 3.50$, $p = 0.003$; all other correlations between FPC and OFC were non-significant, rs <0.04, ps > 0.10).

Collectively, results from (a) the whole-brain searchlight analysis, (b) the hippocampal multivariate-univariate connectivity analysis, and (c) post-hoc classification and representational connectivity correlation analyses highlight a role for OFC in a hippocampal network that codes for prospective goals, and underscore an important role for FPC in putative top-down modulation of hippocampal coding during prospective planning. While the ability to decode representations of specific goal states from FPC may be limited, the findings from both the univariate and representational connectivity analyses suggest that the computations in this region could influence both hippocampal and OFC representations that underlie memory-guided planning.

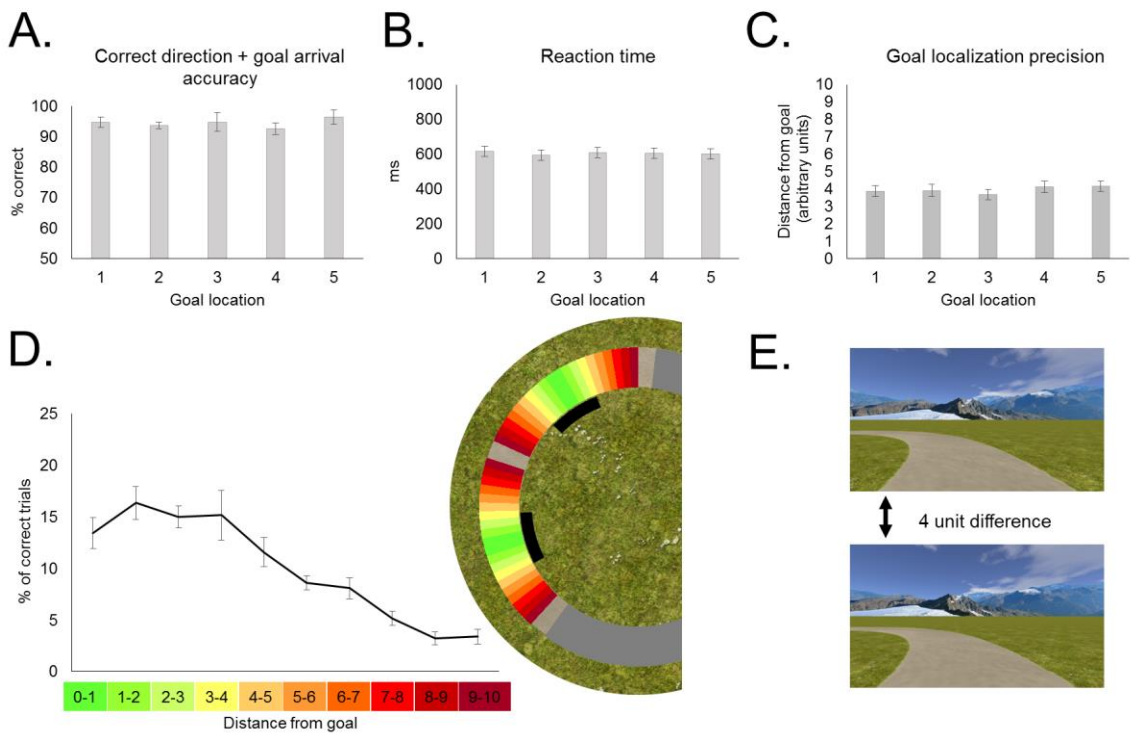

Fig. S1: **A.** Overall navigation performance (correct direction and goal localization) by goal. **B.** Reaction times for selecting the navigational direction following cued planning. **C.** Mean precision at localizing goal locations. **D.** At left: Group precision distribution, plotted as percentage of trials in which participants stopped N virtual units from the precise goal location. Ranges on x-axis reflect distances inclusive of the first value and exclusive of the second (e.g., [0,1)). At right: X-axis precision ranges between two goal locations are color coded on a schematized overhead map of the environment. The darkest shade of red (9-10 units) represents the distal boundary of a given goal location's 10-unit radius quintile. Black bars on map inset visualize the group's mean precision in space. Note that goal locations were further separated by a mean of 2 units (tan space between goal quintiles on track), but the exact separation was jittered across locations and participants. A-D: Error bars reflect the group SEM. **E.** Illustration of perceptual difference at a distance of 4 virtual units (> mean precision error).

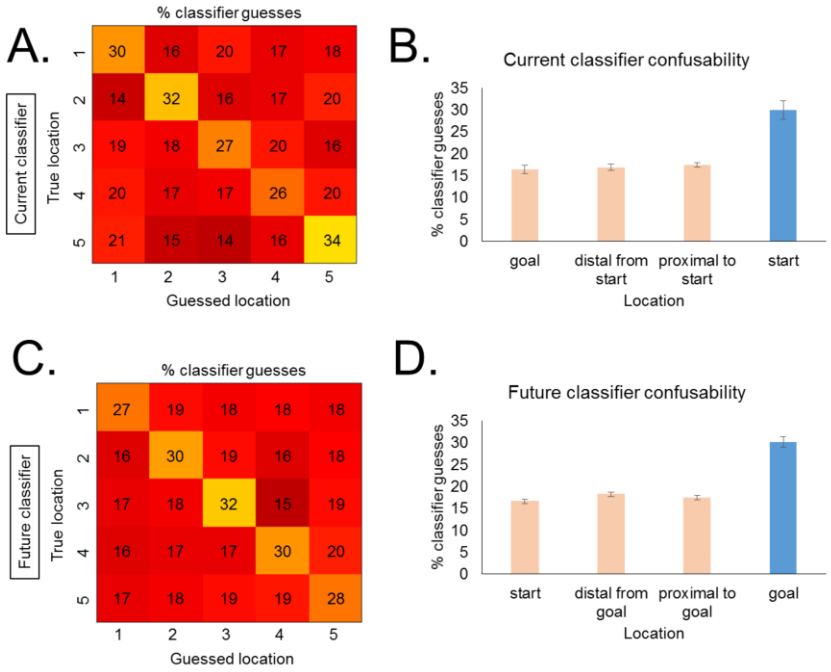

Fig. S2: **A.** Group-level *current* classifier confusion matrix. **B.** *Current* classifier confusion, across all correct navigation trials, sorted by spatial relationship of locations. **C.** Group-level *future* goal classifier confusion matrix. **D.** *Future* classifier confusion, across all correct navigation trials, sorted by spatial relationship of locations. Error bars reflect the group SEM.

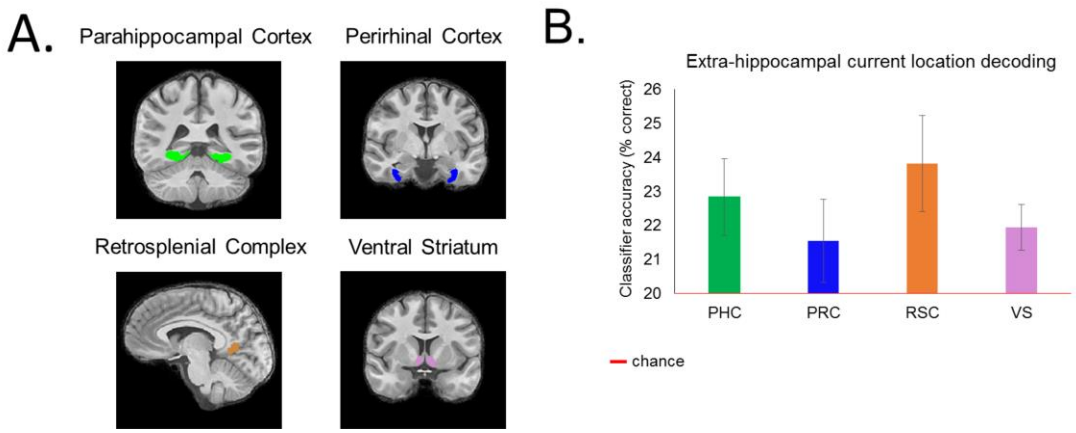

Fig. S3: **A.** Representative manual segmentations of targeted extra-hippocampal regions of interest. **B.** Current location decoding in these targeted cortical regions. Error bars reflect the group SEM.

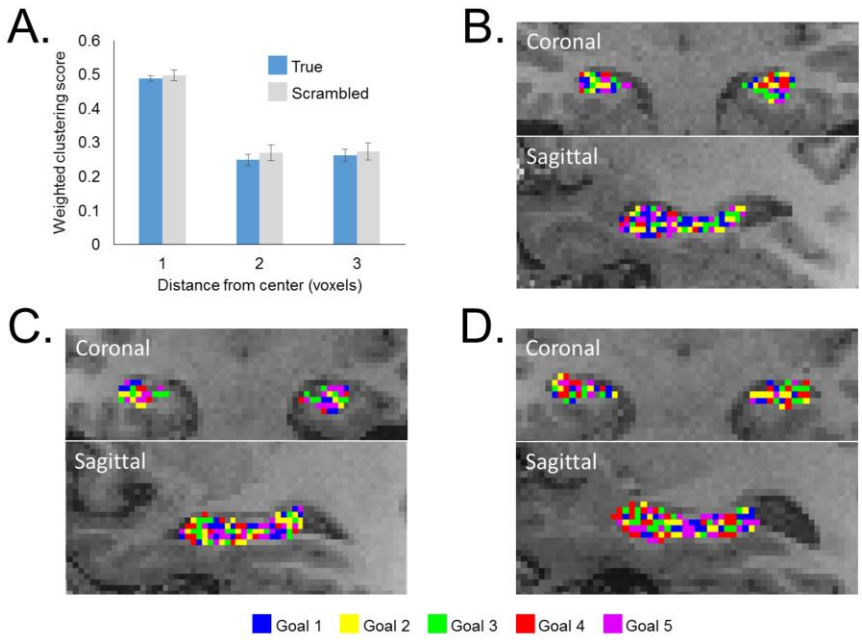

Fig. S4: **A.** Hippocampal location clustering scores for True and Scrambled (baseline) data, plotted by distance (radius, in voxels) from the center voxel of each searchlight. No evidence for location clustering was observed above that expected from the inherent smoothness in empirically established baseline data. Error bars reflect the group SEM. **B-D.** Representative univariate location preference maps from three participants, with clustering scores that ranged from the minimum (B) to the maximum (D) across the sample. Goal location color legend is provided below maps.

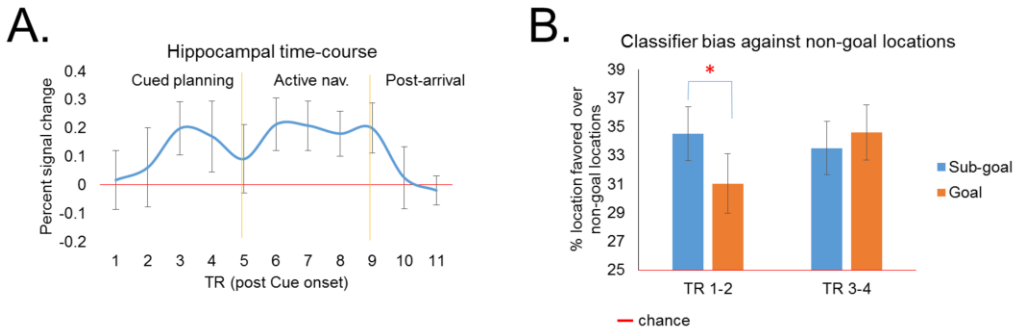

Fig. S5: **A.** Univariate activation time-course extracted from the bilateral hippocampal ROI. Time-course was estimated with an FIR model, using only a cue period onset regressor to allow for visualization of how percent signal change varies across task phases. **B.** Classifier accuracy for TRs 1-2 and 3-4 measured as confusability against remaining non-goal locations. Error bars reflect the group SEM.

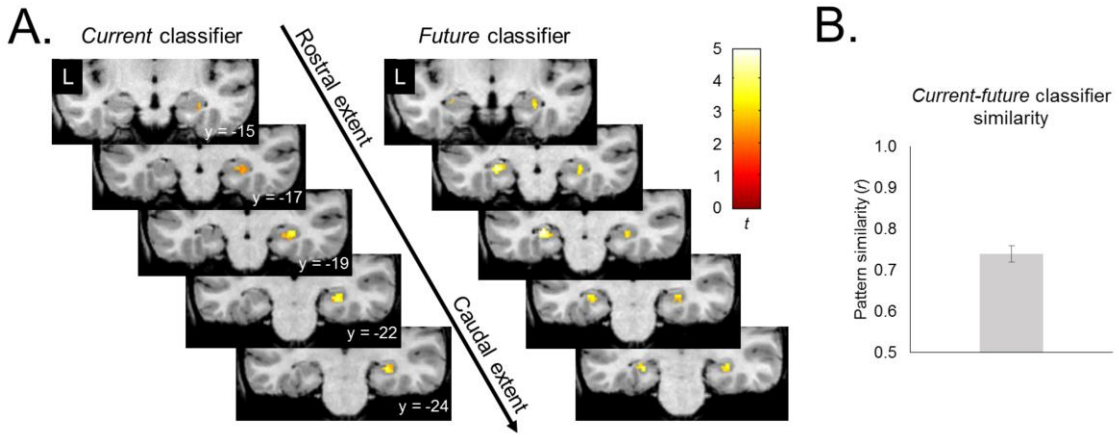

Fig. S6: **A.** *Current* and *future* classifier hippocampal ROI searchlight maps. **B.** Mean pattern similarity (*r*, individual participant level) between unthresholded *current* and *future* classifier maps. Error bars reflect the group SEM.

References and Notes

1. D. L. Schacter, D. R. Addis, On the nature of medial temporal lobe contributions to the constructive simulation of future events. *Philos. Trans. R. Soc. Lond. B Biol. Sci.* **364**, 1245–1253 (2009). Medline doi:10.1098/rstb.2008.0308

2. R. L. Buckner, D. C. Carroll, Self-projection and the brain. *Trends Cogn. Sci.* **11**, 49–57 (2007). Medline doi:10.1016/j.tics.2006.11.004

3. E. R. Wood, P. A. Dudchenko, R. J. Robitsek, H. Eichenbaum, Hippocampal neurons encode information about different types of memory episodes occurring in the same location. *Neuron* **27**, 623–633 (2000). Medline doi:10.1016/S0896-6273(00)00071-4

4. I. Lee, A. L. Griffin, E. A. Zilli, H. Eichenbaum, M. E. Hasselmo, Gradual translocation of spatial correlates of neuronal firing in the hippocampus toward prospective reward locations. *Neuron* **51**, 639–650 (2006). Medline doi:10.1016/j.neuron.2006.06.033

5. D. M. Smith, S. J. Mizumori, Learning-related development of context-specific neuronal responses to places and events: The hippocampal role in context processing. *J. Neurosci.* **26**, 3154–3163 (2006). Medline doi:10.1523/JNEUROSCI.3234-05.2006

6. H. T. Ito, S.-J. Zhang, M. P. Witter, E. I. Moser, M.-B. Moser, A prefrontal-thalamo-hippocampal circuit for goal-directed spatial navigation. *Nature* **522**, 50–55 (2015). Medline doi:10.1038/nature14396

7. J. Ferbinteanu, M. L. Shapiro, Prospective and retrospective memory coding in the hippocampus. *Neuron* **40**, 1227–1239 (2003). Medline doi:10.1016/S0896-6273(03)00752-9

8. T. I. Brown, M. E. Hasselmo, C. E. Stern, A high-resolution study of hippocampal and medial temporal lobe correlates of spatial context and prospective overlapping route memory. *Hippocampus* **24**, 819–839 (2014). Medline doi:10.1002/hipo.22273

9. T. I. Brown, C. E. Stern, Contributions of medial temporal lobe and striatal memory systems to learning and retrieving overlapping spatial memories. *Cereb. Cortex* **24**, 1906–1922 (2014). Medline doi:10.1093/cercor/bht041

10. T. I. Brown, R. S. Ross, J. B. Keller, M. E. Hasselmo, C. E. Stern, Which way was I going? Contextual retrieval supports the disambiguation of well learned overlapping navigational routes. *J. Neurosci.* **30**, 7414–7422 (2010). Medline doi:10.1523/JNEUROSCI.6021-09.2010

11. T. I. Brown, R. S. Ross, S. M. Tobyne, C. E. Stern, Cooperative interactions between hippocampal and striatal systems support flexible navigation. *Neuroimage* **60**, 1316–1330 (2012). Medline doi:10.1016/j.neuroimage.2012.01.046

12. T. I. Brown, A. S. Whiteman, I. Aselcioglu, C. E. Stern, Structural differences in hippocampal and prefrontal gray matter volume support flexible context-dependent navigation ability. *J. Neurosci.* **34**, 2314–2320 (2014). Medline doi:10.1523/JNEUROSCI.2202-13.2014

13. M. E. Hasselmo, H. Eichenbaum, Hippocampal mechanisms for the context-dependent retrieval of episodes. *Neural Netw.* **18**, 1172–1190 (2005). Medline doi:10.1016/j.neunet.2005.08.007

14. M. E. Hasselmo, A model of episodic memory: Mental time travel along encoded trajectories using grid cells. *Neurobiol. Learn. Mem.* **92**, 559–573 (2009). Medline doi:10.1016/j.nlm.2009.07.005

15. M. E. Hasselmo, C. E. Stern, Theta rhythm and the encoding and retrieval of space and time. *Neuroimage* **85**, 656–666 (2014). Medline doi:10.1016/j.neuroimage.2013.06.022

16. A. Johnson, A. D. Redish, Neural ensembles in CA3 transiently encode paths forward of the animal at a decision point. *J. Neurosci.* **27**, 12176–12189 (2007). Medline doi:10.1523/JNEUROSCI.3761-07.2007

17. A. M. Wikenheiser, A. D. Redish, Hippocampal theta sequences reflect current goals. *Nat. Neurosci.* **18**, 289–294 (2015). Medline doi:10.1038/nn.3909

18. D. R. Addis, A. T. Wong, D. L. Schacter, Remembering the past and imagining the future: Common and distinct neural substrates during even construction and elaboration. *Neuropsychologia* **45**, 1363–1377 (2007). doi:10.1016/j.neuropsychologia.2006.10.016

19. M. A. A. van der Meer, A. Johnson, N. C. Schmitzer-Torbert, A. D. Redish, Triple dissociation of information processing in dorsal striatum, ventral striatum, and hippocampus on a learned spatial decision task. *Neuron* **67**, 25–32 (2010). Medline doi:10.1016/j.neuron.2010.06.023

20. P. Byrne, S. Becker, N. Burgess, Remembering the past and imagining the future: A neural model of spatial memory and imagery. *Psychol. Rev.* **114**, 340–375 (2007). Medline doi:10.1037/0033-295X.114.2.340

21. N. Burgess, S. Becker, J. A. King, J. O'Keefe, Memory for events and their spatial context: Models and experiments. *Philos. Trans. R. Soc. Lond. B Biol. Sci.* **356**, 1493–1503 (2001). Medline doi:10.1098/rstb.2001.0948

22. N. Ramnani, A. M. Owen, Anterior prefrontal cortex: Insights into function from anatomy and neuroimaging. *Nat. Rev. Neurosci.* **5**, 184–194 (2004). Medline doi:10.1038/nrn1343

23. H. J. Spiers, S. J. Gilbert, Solving the detour problem in navigation: A model of prefrontal and hippocampal interactions. *Front. Hum. Neurosci.* **9**, 125 (2015). Medline doi:10.3389/fnhum.2015.00125

24. J. F. Miller, M. Neufang, A. Solway, A. Brandt, M. Trippel, I. Mader, S. Hefft, M. Merkow, S. M. Polyn, J. Jacobs, M. J. Kahana, A. Schulze-Bonhage, Neural activity in human hippocampal formation reveals the spatial context of retrieved memories. *Science* **342**, 1111–1114 (2013). Medline doi:10.1126/science.1244056

25. A. D. Ekstrom, M. J. Kahana, J. B. Caplan, T. A. Fields, E. A. Isham, E. L. Newman, I. Fried, Cellular networks underlying human spatial navigation. *Nature* **425**, 184–188 (2003). Medline doi:10.1038/nature01964

26. L. R. Howard, A. H. Javadi, Y. Yu, R. D. Mill, L. C. Morrison, R. Knight, M. M. Loftus, L. Staskute, H. J. Spiers, The hippocampus and entorhinal cortex encode the path and Euclidean distances to goals during navigation. *Curr. Biol.* **24**, 1331–1340 (2014). Medline doi:10.1016/j.cub.2014.05.001

27. K. R. Sherrill, U. M. Erdem, R. S. Ross, T. I. Brown, M. E. Hasselmo, C. E. Stern, Hippocampus and retrosplenial cortex combine path integration signals for successful navigation. *J. Neurosci.* **33**, 19304–19313 (2013). Medline doi:10.1523/JNEUROSCI.1825-13.2013

28. H. J. Spiers, E. A. Maguire, A navigational guidance system in the human brain. *Hippocampus* **17**, 618–626 (2007). Medline doi:10.1002/hipo.20298

29. C. F. Doeller, C. Barry, N. Burgess, Evidence for grid cells in a human memory network. *Nature* **463**, 657–661 (2010). Medline doi:10.1038/nature08704

30. M. J. Chadwick, A. E. J. Jolly, D. P. Amos, D. Hassabis, H. J. Spiers, A goal direction signal in the human entorhinal/subicular region. *Curr. Biol.* **25**, 87–92 (2015). Medline doi:10.1016/j.cub.2014.11.001

31. V. Sulpizio, G. Committeri, G. Galati, Distributed cognitive maps reflecting real distances between places and views in the human brain. *Front. Hum. Neurosci.* **8**, 716 (2014). Medline doi:10.3389/fnhum.2014.00716

32. D. Hassabis, C. Chu, G. Rees, N. Weiskopf, P. D. Molyneux, E. A. Maguire, Decoding neuronal ensembles in the human hippocampus. *Curr. Biol.* **19**, 546–554 (2009). Medline doi:10.1016/j.cub.2009.02.033

33. S. A. Marchette, L. K. Vass, J. Ryan, R. A. Epstein, Anchoring the neural compass: Coding of local spatial reference frames in human medial parietal lobe. *Nat. Neurosci.* **17**, 1598–1606 (2014). Medline doi:10.1038/nn.3834

34. S. A. Marchette, L. K. Vass, J. Ryan, R. A. Epstein, Outside looking in: Landmark generalization in the human navigational system. *J. Neurosci.* **35**, 14896–14908 (2015). Medline doi:10.1523/JNEUROSCI.2270-15.2015

35. S. McKenzie, N. T. M. Robinson, L. Herrera, J. C. Churchill, H. Eichenbaum, Learning causes reorganization of neuronal firing patterns to represent related experiences within a hippocampal schema. *J. Neurosci.* **33**, 10243–10256 (2013). Medline doi:10.1523/JNEUROSCI.0879-13.2013

36. J. C. Liang, A. D. Wagner, A. R. Preston, Content representation in the human medial temporal lobe. *Cereb. Cortex* **23**, 80–96 (2013). Medline doi:10.1093/cercor/bhr379

37. E. M. Aminoff, K. Kveraga, M. Bar, The role of the parahippocampal cortex in cognition. *Trends Cogn. Sci.* **17**, 379–390 (2013). Medline doi:10.1016/j.tics.2013.06.009

38. R. Navawongse, H. Eichenbaum, Distinct pathways for rule-based retrieval and spatial mapping of memory representations in hippocampal neurons. *J. Neurosci.* **33**, 1002–1013 (2013). Medline doi:10.1523/JNEUROSCI.3891-12.2013

39. H. Barbas, G. J. Blatt, Topographically specific hippocampal projections target functionally distinct prefrontal areas in the rhesus monkey. *Hippocampus* **5**, 511–533 (1995). Medline doi:10.1002/hipo.450050604

40. T. Wolbers, J. M. Wiener, Challenges for identifying the neural mechanisms that support spatial navigation: The impact of spatial scale. *Front. Hum. Neurosci.* **8**, 571 (2014). Medline doi:10.3389/fnhum.2014.00571

41. D. A. Feinberg, S. Moeller, S. M. Smith, E. Auerbach, S. Ramanna, M. Gunther, M. F. Glasser, K. L. Miller, K. Ugurbil, E. Yacoub, Multiplexed echo planar imaging for sub-second whole brain FMRI and fast diffusion imaging. *PLOS ONE* **5**, e15710 (2010). Medline doi:10.1371/journal.pone.0015710

42. K. Setsompop, B. A. Gagoski, J. R. Polimeni, T. Witzel, V. J. Wedeen, L. L. Wald, Blipped-controlled aliasing in parallel imaging for simultaneous multislice echo planar imaging with reduced g-factor penalty. *Magn. Reson. Med.* **67**, 1210–1224 (2012). Medline doi:10.1002/mrm.23097

43. J. L. Andersson, C. Hutton, J. Ashburner, R. Turner, K. Friston, Modeling geometric deformations in EPI time series. *Neuroimage* **13**, 903–919 (2001). Medline doi:10.1006/nimg.2001.0746

44. R. Insausti, K. Juottonen, H. Soininen, A. M. Insausti, K. Partanen, P. Vainio, M. P. Laakso, A. Pitkänen, MR volumetric analysis of the human entorhinal, perirhinal, and temporopolar cortices. *AJNR Am. J. Neuroradiol.* **19**, 659–671 (1998). Medline

45. J. C. Pruessner, L. M. Li, W. Serles, M. Pruessner, D. L. Collins, N. Kabani, S. Lupien, A. C. Evans, Volumetry of hippocampus and amygdala with high-resolution MRI and three-dimensional analysis software: Minimizing the discrepancies between laboratories. *Cereb. Cortex* **10**, 433–442 (2000). Medline doi:10.1093/cercor/10.4.433

46. J. C. Pruessner, S. Köhler, J. Crane, M. Pruessner, C. Lord, A. Byrne, N. Kabani, D. L. Collins, A. C. Evans, Volumetry of temporopolar, perirhinal, entorhinal and parahippocampal cortex from high-resolution MR images: Considering the variability of the collateral sulcus. *Cereb. Cortex* **12**, 1342–1353 (2002). Medline doi:10.1093/cercor/12.12.1342

47. M. M. Zeineh, S. A. Engel, S. Y. Bookheimer, Application of cortical unfolding techniques to functional MRI of the human hippocampal region. *Neuroimage* **11**, 668–683 (2000). Medline doi:10.1006/nimg.2000.0561

48. H. M. Duvernoy, *The Human Hippocampus: Functional Anatomy, Vascularization and Serial Sections with MRI* (Springer, 2005).

49. A. R. Preston, A. M. Bornstein, J. B. Hutchinson, M. E. Gaare, G. H. Glover, A. D. Wagner, High-resolution fMRI of content-sensitive subsequent memory responses in human medial temporal lobe. *J. Cogn. Neurosci.* **22**, 156–173 (2010). Medline doi:10.1162/jocn.2009.21195

50. H. C. Breiter, R. L. Gollub, R. M. Weisskoff, D. N. Kennedy, N. Makris, J. D. Berke, J. M. Goodman, H. L. Kantor, D. R. Gastfriend, J. P. Riorden, R. T. Mathew, B. R. Rosen, S. E. Hyman, Acute effects of cocaine on human brain activity and emotion. *Neuron* **19**, 591–611 (1997). Medline doi:10.1016/S0896-6273(00)80374-8

51. J. Ashburner, A fast diffeomorphic image registration algorithm. *Neuroimage* **38**, 95–113 (2007). Medline doi:10.1016/j.neuroimage.2007.07.007

52. P. E. Sharp, C. Green, Spatial correlates of firing patterns of single cells in the subiculum of the freely moving rat. *J. Neurosci.* **14**, 2339–2356 (1994). Medline

53. N. Burgess, J. O'Keefe, Neuronal computations underlying the firing of place cells and their role in navigation. *Hippocampus* **6**, 749–762 (1996). Medline doi:10.1002/(SICI)1098-1063(1996)6:6<749::AID-HIPO16>3.0.CO;2-0

54. N. Kriegeskorte, R. Goebel, P. Bandettini, Information-based functional brain mapping. *Proc. Natl. Acad. Sci. U.S.A.* **103**, 3863–3868 (2006). Medline doi:10.1073/pnas.0600244103

55. P. F. Rodriguez, Neural decoding of goal locations in spatial navigation in humans with fMRI. *Hum. Brain Mapp.* **31**, 391–397 (2010). Medline

56. N. Tzourio-Mazoyer, B. Landeau, D. Papathanassiou, F. Crivello, O. Etard, N. Delcroix, B. Mazoyer, M. Joliot, Automated anatomical labeling of activations in SPM using a macroscopic anatomical parcellation of the MNI MRI single-subject brain. *Neuroimage* **15**, 273–289 (2002). Medline doi:10.1006/nimg.2001.0978

57. J. A. Maldjian, P. J. Laurienti, J. H. Burdette, Precentral gyrus discrepancy in electronic versions of the Talairach atlas. *Neuroimage* **21**, 450–455 (2004). Medline doi:10.1016/j.neuroimage.2003.09.032

58. J. A. Maldjian, P. J. Laurienti, R. A. Kraft, J. H. Burdette, An automated method for neuroanatomic and cytoarchitectonic atlas-based interrogation of fMRI data sets. *Neuroimage* **19**, 1233–1239 (2003). Medline doi:10.1016/S1053-8119(03)00169-1